

Trends in atmospheric patterns conducive to seasonal precipitation and temperature extremes in California

Daniel L. Swain,^{1,*} Daniel E. Horton,^{1,2} Deepti Singh,^{1,3} Noah S. Diffenbaugh^{1,4}

Recent evidence suggests that changes in atmospheric circulation have altered the probability of extreme climate events in the Northern Hemisphere. We investigate northeastern Pacific atmospheric circulation patterns that have historically (1949–2015) been associated with cool-season (October–May) precipitation and temperature extremes in California. We identify changes in occurrence of atmospheric circulation patterns by measuring the similarity of the cool-season atmospheric configuration that occurred in each year of the 1949–2015 period with the configuration that occurred during each of the five driest, wettest, warmest, and coolest years. Our analysis detects statistically significant changes in the occurrence of atmospheric patterns associated with seasonal precipitation and temperature extremes. We also find a robust increase in the magnitude and subseasonal persistence of the cool-season West Coast ridge, resulting in an amplification of the background state. Changes in both seasonal mean and extreme event configurations appear to be caused by a combination of spatially nonuniform thermal expansion of the atmosphere and reinforcing trends in the pattern of sea level pressure. In particular, both thermal expansion and sea level pressure trends contribute to a notable increase in anomalous northeastern Pacific ridging patterns similar to that observed during the 2012–2015 California drought. Collectively, our empirical findings suggest that the frequency of atmospheric conditions like those during California's most severely dry and hot years has increased in recent decades, but not necessarily at the expense of patterns associated with extremely wet years.

INTRODUCTION

Persistent and/or recurring atmospheric circulation anomalies are strongly linked to surface meteorological extremes (1). Such atmospheric patterns can lead to high-impact weather and climate events across a wide range of temporal and spatial scales, from localized flash flooding caused by single-day slow-moving convective downpours to continental-scale droughts associated with multidecadal oceanic oscillations. Regions with relatively short or sharply defined wet seasons—where there is limited potential for meaningful precipitation during the canonical dry season—may be particularly susceptible to the hydroclimatic effects of unusually long-lived circulation anomalies that persist (or recur) across seasonal to annual scales. Here, anomalous circulation patterns that disrupt or enhance typical precipitation-generating mechanisms for several consecutive months can have disproportionately large effects on total annual precipitation and, consequently, on subsequent drought or flood risk [for example, Wise and Dannenberg (2)]. For drought risk in particular, this effect may be further amplified where the dry season coincides with the warm season because high temperatures increase net water stress by heightening potential evapotranspirative demand (3).

The state of California provides an important example of societal and ecological vulnerability to hydroclimatic extremes. California is home to nearly 39 million people (4), has the eighth largest economy in the world (5), and is an agricultural center of national and international significance (6). It is also considered to be a global biodiversity hotspot (7) and contains 49 million acres of protected forests and parklands (8). This socioeconomically and geographically complex region

receives the vast majority (~95%) of its annual precipitation in the form of rain and high-elevation snow between the cool-season months of October and May, including ~66% during the core rainy season months from December to March [data from the NOAA National Climatic Data Center (NCDC) at www.ncdc.noaa.gov/cag]. Nearly all of this precipitation occurs during the passage of extratropical cyclonic systems from late autumn to early spring (9), with a much smaller fraction falling as the result of warm-season deep convection associated with the westernmost fringe of the North American Monsoon (10). Because the state lies near (and often to the south of) the wintertime polar jet stream and the prevailing North Pacific storm track, the large relative contribution to total annual precipitation by short-duration periods of storm activity associated with transient southward shifts in the jet stream is unique in a North American context (11, 12). Moreover, recent work has shown that the occurrence (or absence) of individual extreme precipitation events associated with East Pacific “atmospheric rivers”—which typically occur only a handful of times each rainy season—can often “make or break” California’s precipitation total for the entire year (12). Given this combination of socioeconomic, ecological, and climatological characteristics, California and the adjacent northeastern Pacific Ocean make for a compelling test bed in which to explore large-scale atmospheric circulation patterns associated with regional climate extremes.

California’s ongoing multiyear drought (2012–2015), which by many metrics is the most severe in the direct instrumental record (13–17)—and perhaps in a millennium or more (13, 15)—provides additional motivation for this investigation (18). The extremely low precipitation and extremely high temperatures associated with the current California drought stem from the persistent northward deflection of the cool-season storm track by a recurring anomalous anticyclone over the

2016 © The Authors, some rights reserved;
exclusive licensee American Association for
the Advancement of Science. Distributed
under a Creative Commons Attribution
NonCommercial License 4.0 (CC BY-NC).
10.1126/sciadv.1501344

¹Department of Earth System Science, Stanford University, Stanford, CA 94305, USA. ²Department of Earth and Planetary Sciences, Northwestern University, Evanston, IL 60208, USA. ³Lamont-Doherty Earth Observatory, Columbia University, Palisades, NY 10964, USA. ⁴Woods Institute for the Environment, Stanford University, Stanford, CA 94305, USA.

*Corresponding author. E-mail: dlswain@stanford.edu

far northeastern Pacific (nicknamed the “Ridiculously Resilient Ridge” for its extraordinary persistence) (19). The anomalous ridge has not been a static feature; rather, it has exhibited substantial variation in intensity from month to month and a notable eastward shift toward the West Coast over successive winters. However, it has remained a very prominent [and observationally unprecedented (19)] feature in seasonal mean fields for the full duration of the drought [data from the NOAA Earth System Research Laboratory (ESRL) online data plotter at www.esrl.noaa.gov/psd/]. Various mechanistic hypotheses have been posed to account for the persistence of this northeastern Pacific ridge, including (i) remote teleconnections from anomalous warmth in the western tropical Pacific Ocean (20–22) and subsequent extratropical ocean-atmosphere feedbacks (22, 23), (ii) remote teleconnections from negative Arctic sea ice anomalies and direct/indirect thermal effects on the North Pacific geopotential height (GPH) field (22, 24, 25), and (iii) internal (“natural”) atmospheric variability (26). The potential mechanistic role of anthropogenic forcing is less certain, but several studies suggest that human greenhouse gas emissions may have influenced the likelihood of occurrence of a persistent anticyclone in this region, possibly via teleconnections to the western tropical Pacific Ocean and/or Arctic sea ice (19, 20, 22, 27, 28).

Despite uncertainty in the physical causes of this and other high-profile meteorological events (29), it is clear that the Northern Hemisphere has experienced heterogeneous trends in atmospheric circulation in recent decades, and that these trends have influenced the probability of certain kinds of extremes (30). Regardless of whether these atmospheric trends are the result of natural variability or anthropogenic forcings (or some combination of the two), the impacts on natural and human systems have been substantial.

Given California’s intrinsic hydroclimatic sensitivity to seasonally persistent circulation regimes, we restrict our geographic focus to circulation patterns associated with historical statewide precipitation and temperature extremes. We also emphasize that our study focuses on detecting changes in circulation patterns over the period of record, rather than attributing these changes to particular causes. However, the general framework of our analysis can be readily applied to characterizing and detecting changes in other regions of the globe and/or to attributing observed changes to underlying natural or anthropogenic causes.

RESULTS

We analyzed atmospheric reanalysis data to identify changes in atmospheric patterns occurring within the North Pacific domain (NPD; see Materials and Methods). We first considered long-term trends in large-scale atmospheric characteristics (Figs. 1 and 2 and figs. S1 and S2). We then assessed whether there were discernable changes in the occurrence of patterns exhibiting high spatial similarity to those during California’s five driest (Fig. 3 and fig. S3), five wettest (Fig. 4 and fig. S4), five warmest (Fig. 5 and fig. S5), and five coolest years (Fig. 6 and fig. S6) (using raw precipitation data, both raw and detrended GPH data, and detrended temperature data; see Materials and Methods and figs. S7 to S10). Using 500-mb GPH, four of the extreme atmospheric configurations exhibited statistically significant increases in frequency (including 2 dry, 0 wet, 2 warm, and 0 cool), and three atmospheric configurations exhibited statistically significant decreases in frequency (including 1 dry, 0 wet, 1 warm, and 1 cool) (Fig. 1F). Using sea level pressure (SLP), eight atmospheric configurations exhibited statistically significant increases

in frequency (including 1 dry, 4 wet, 3 warm, and 0 cool), and one atmospheric configuration exhibited statistically significant decreases in frequency (0 dry, 0 wet, 1 warm, and 0 cool) (Fig. 1G). Notably, GPH and SLP patterns from 2 years during California’s ongoing severe drought showed large and statistically significant increases in frequency: 2013–2014 (extreme dry; Fig. 3E and fig. S3E) and 2014–2015 (extreme warm; Fig. 5E and fig. S5E). Also, whereas none of the GPH patterns associated with California’s five wettest years exhibited statistically significant changes (Fig. 1F)—including 1982–1983 (Fig. 4C) and 1997–1998 (Fig. 4E), which were associated with the two strongest El Niño events in the observed record—four of five corresponding “wet” SLP patterns showed a statistically significant increase in frequency (Fig. 1G).

To verify that moderate to high positive pattern correlations were meaningful predictors of surface weather extremes in California, we assessed the categorization skill for each “year type” (that is, dry/wet/warm/cool) (Fig. 1E and fig. S7). We found that moderate to high positive GPH pattern correlation correctly identified increased probability (in a given year) of anomalous precipitation/temperature conditions associated with four of five dry patterns, five of five wet patterns, three of five warm patterns, and four of five cool patterns (Fig. 1E). Likewise, SLP pattern correlation correctly identified the increased probability of anomalous precipitation/temperature conditions associated with four of five dry patterns, four of five wet patterns, two of five warm patterns, and three of five cool patterns (Fig. 1E). These results confirm that NPD GPH and SLP pattern correlations indeed provide useful information regarding the likelihood of surface meteorological extremes in California, although SLP correlations are generally less skillful than GPH for temperature extremes (Fig. 1E). The magnitude and statistical significance of changes in the frequency of years with high pattern correlation often exceeded that which might be inferred from the mean linear trend in correlation alone, especially for SLP (Fig. 1, F and G, and figs. 3 to 6). This finding highlights the importance of focusing on highly correlated patterns when assessing changes in relatively uncommon or extreme atmospheric configurations.

The NPD spans a large geographic region and encompasses both the cool-season storm development region near the Aleutian Islands/Gulf of Alaska and the climatological mean West Coast ridge (Fig. 1, A to C). We therefore also considered changes in the mean October–May zonal gradient in GPH because this gradient is an indicator of broad-scale changes in the storm track. We found increasing trends in the zonal GPH gradient in the NPD in all four latitude bands, which were statistically significant in all but the northernmost band (Fig. 1D). Further, we found that the occurrence of high gradient years increased in all four latitude bands between the 1949–1981 and 1982–2015 periods, whereas the occurrence of low gradient years decreased in all four latitude bands (Fig. 2C). The increase in the mean gradient between these two periods was statistically significant in the middle two latitude bands (30°N–40°N and 40°N–50°N) (Fig. 2, A and B), which are directly west of California and are therefore highly relevant for California meteorological extremes.

We also assessed changes in the zonal GPH gradient at subseasonal (monthly) time scales. We found a large number of individual calendar months during which the zonal gradient demonstrated a statistically significant increase (mostly during winter and spring), particularly in the 30°N–40°N [4 of 8 months (Fig. 2A)] and 40°N–50°N [4 of 8 months (Fig. 2B)] bands. For the 30°N–40°N band, this shift represented a notable amplification of the well-defined preexisting seasonal cycle, with the largest positive increases in the gradient coinciding with the calendar

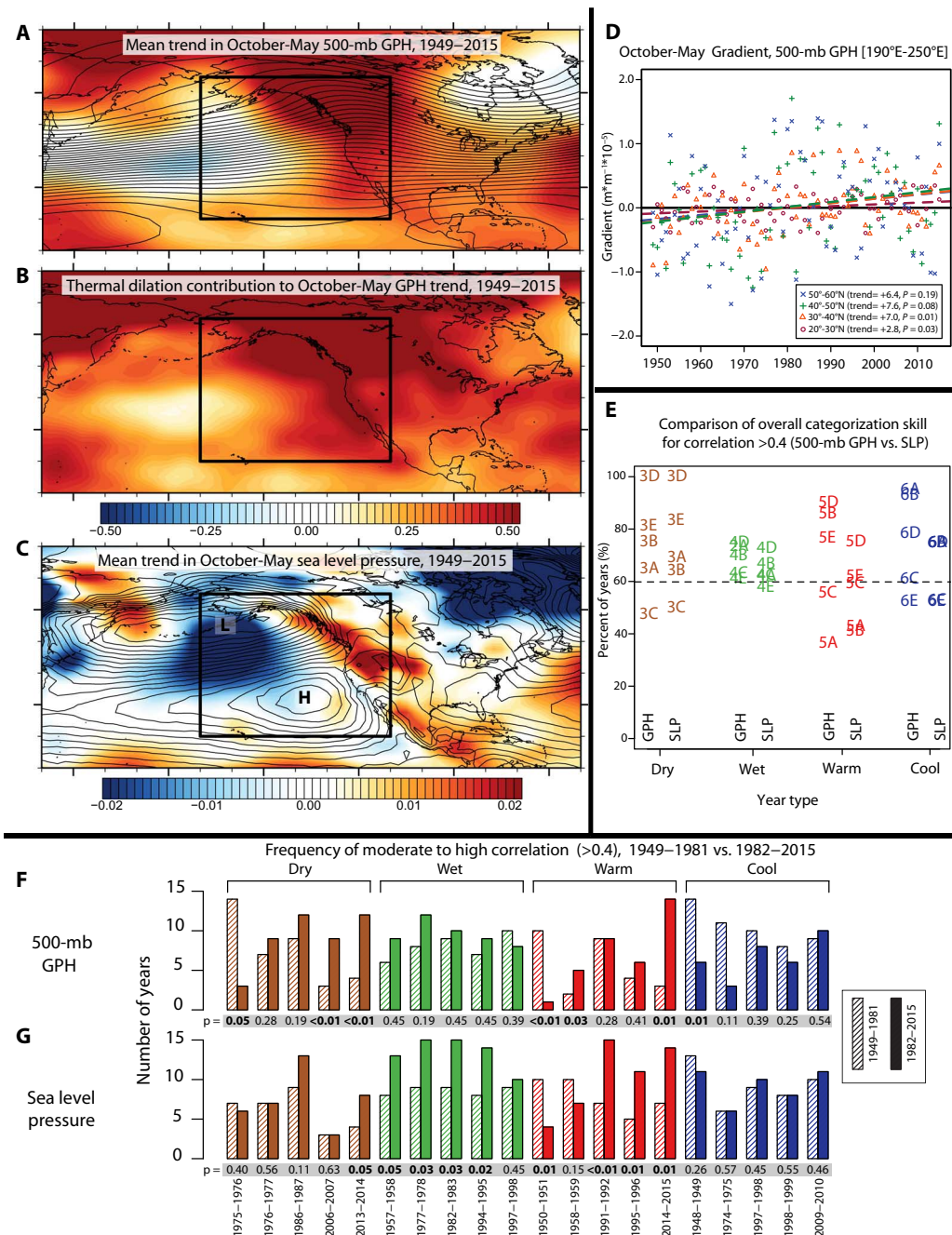


Fig. 1. Observed October-May changes across the northeastern Pacific. (A) Mean trend in October-May 500-mb GPH over the northeastern Pacific and western North America, 1949–2015 (meters per year). (B) Contribution of lower tropospheric warming (thermal dilation) to observed October-May GPH trend (meters per year). (C) Mean trend in October-May SLP over the northeastern Pacific and western North America, 1949–2015 (millibars per year). Black box in (A) to (C) depicts the NPD. (D) Time series of mean October-May zonal gradient of 500-mb GPH in the NPD over four separate latitude bands (10^{-5} m/m). Units of reported trends are 10^{-8} m/(m \cdot y). (E) Predictive skill of moderate to high pattern correlation using GPH and SLP. The quantity plotted is the percent of years that exhibited a pattern correlation of >0.4 with a particular extreme pattern and also experienced surface meteorological conditions of the correct sign (for example, low precipitation in a year that also had high correlation with one of the five dry patterns). Dashed horizontal line at 60% represents threshold for defining “increased likelihood” of a precipitation or temperature anomaly of the correct sign (as described in the text). Labels correspond to specific GPH/SLP patterns shown in matching figure panels in Figs. 3 to 6 [for example, “3D” corresponds to (D) in Fig. 3]. (F) Changes in the occurrence of GPH patterns that have moderate to high correlation (>0.4) with patterns of interest (that is, those associated with surface meteorological extremes). Left columns (striped fill) represent the 1949–1981 occurrence; right columns (solid fill) represent the 1982–2015 occurrence. Numbers in the gray horizontal rectangle under the column pairs indicate confidence (P) values that the change is statistically significant. (G) Same as in (F) but for SLP patterns.

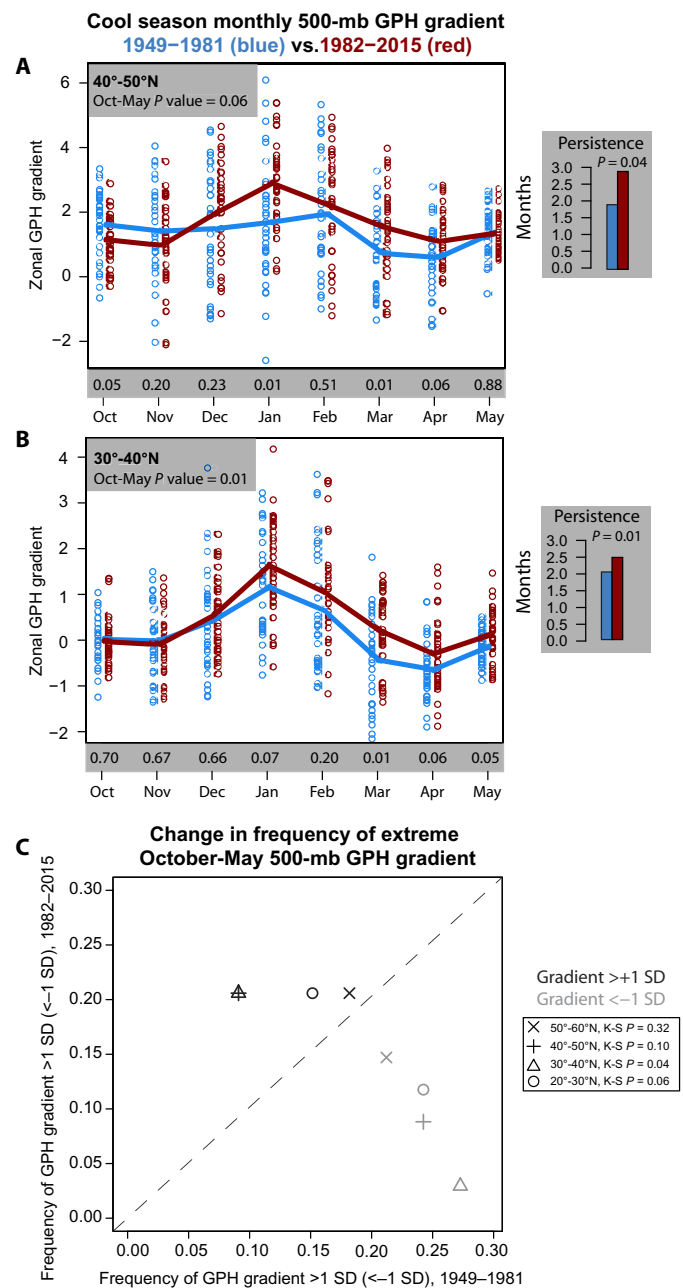


Fig. 2. Observed October–May changes in zonal GPH gradient over the northeastern Pacific. Blue (red) points represent monthly values of the west-to-east GPH gradient averaged over the given range of latitudes from each year of the 1949–1981 (1982–2015) period. (A and B) Blue (red) curves represent monthly values of the west-to-east GPH gradient averaged over the given range of latitudes, averaged over 1949–1981 (1982–2015). The gray rectangles to the right of each panel show the change in subseasonal persistence of GPH gradients above the long-term average (months per year). Blue (red) columns represent mean values for 1949–1981 (1982–2015). (C) Change in extreme (± 1 SD) 500-mb NPD GPH gradients between 1949–1981 and 1982–2015 over four separate latitude bands. Points above the dashed 1:1 line imply increasing frequency; points below 1:1 line imply decreasing frequency.

months in which the gradient reaches its climatological maximum (Fig. 2, A and B).

In addition to these increases in the mean zonal GPH gradient at the seasonal and monthly scale, we also found a statistically significant increase in the subseasonal (month-to-month) persistence of anomalously high gradients (Fig. 2 and fig. S2, insets). This is especially noteworthy given the importance of recurring and/or persistent circulation anomalies in generating California precipitation extremes (31, 32). Increases in the magnitude and persistence of strongly positive zonal GPH gradients acted to reinforce the West Coast cool-season mean ridge (Fig. 1A), amplifying the climatological mean midtropospheric wave pattern and displacing the Pacific jet stream (and associated storm activity) to the north of California (19). This last finding of increased persistence of high GPH gradients therefore has particular relevance for drought in California and supports our findings of increased frequency of atmospheric patterns similar to those experienced during California’s driest and warmest years (Fig. 1, F and G).

Observed increases in the NPD GPH gradient (mean and extreme values; Fig. 2) and in the GPH itself (Fig. 1A) were spatially coincident with trends of the same sign in both lower tropospheric thermal expansion (dilation) (Fig. 1B) and SLP (Fig. 1C). Whereas the magnitude of the thermal dilation trend was considerably larger than that of the SLP trend, both were positive (and, indeed, had local maxima) near the axis of the West Coast mean ridge (Fig. 1A). Thus, this reinforcing pattern of positive thermal dilation and positive SLP changes appears to contribute to the observed increase in cool-season mean ridge amplitude (Fig. 1A) and resembles certain specific extreme event configurations that have exhibited increasing occurrence (Fig. 1, F and G)—especially anomalous northeastern Pacific ridging patterns similar to those observed during the 2012–2015 California drought (Figs. 3E and 5E).

DISCUSSION

Contribution of circulation changes to California’s cool-season precipitation extremes

Careful consideration of the specific GPH/SLP patterns observed during extreme wet and dry years yields further insights. GPH and SLP patterns during extreme wet years exhibit a high degree of homogeneity in the NPD, with a broad region of negative anomalies west of California occurring during each of California’s five wettest years (Fig. 4 and fig. S4). In contrast, patterns during extreme dry years exhibit considerable heterogeneity (Fig. 3 and fig. S3) [although four of five dry patterns are characterized by an anomalously positive west-to-east GPH/SLP gradient and anomalously high GPH over California (Fig. 3, B to E, and fig. S3, B to E)]. These structural differences between extreme dry and extreme wet years may indicate asymmetry in underlying dynamical mechanisms. Negative NPD anomalies during extreme wet years spatially coincide with the mean exit region of the Pacific jet stream, which is suggestive of an eastward extension and/or southward shift of the cool-season storm track toward California (33). The west-east negative-positive anomaly that is present during four of five extreme dry years acts to reinforce the climatological cool-season midtropospheric wave pattern, which is characterized by a relative “ridge” roughly aligned with the west coast of North America (Fig. 1A). Such amplification of the cool-season mean state leads to a sharper south-to-north storm track over the northeastern Pacific, causing weather systems originating in the Central Pacific to preferentially veer northward toward

the Pacific Northwest and British Columbia, and thereby miss California (19).

The apparent divergence between GPH- and SLP-based metrics for assessing the change in wet circulation patterns may be a product of thermal dilation because increases in the mean height of the 500-mb GPH surface could mask a simultaneous increase in relative cyclonic anomalies in the middle troposphere. However, we note that the “predictive skill” of pattern correlation using both GPH and SLP is actually quite similar—and relatively high—for both wet and dry extremes (Fig. 1E). We find a corresponding increase in the actual occurrence

of October–May periods experiencing very high (>80th percentile) and very low (<20th percentile) precipitation, although neither of these increases is statistically significant. (The frequency of wet years increases from 18.2 to 23.5% between 1949–1981 and 1982–2015, and the frequency of dry years increases from 18.2 to 26.5%.) We suggest that GPH- and/or SLP-based measures of changes in large-scale circulation over the North Pacific may be subject to less background variability than California precipitation itself, and therefore may offer the potential for earlier detection of 21st century changes in California’s hydroclimatology (34, 35).

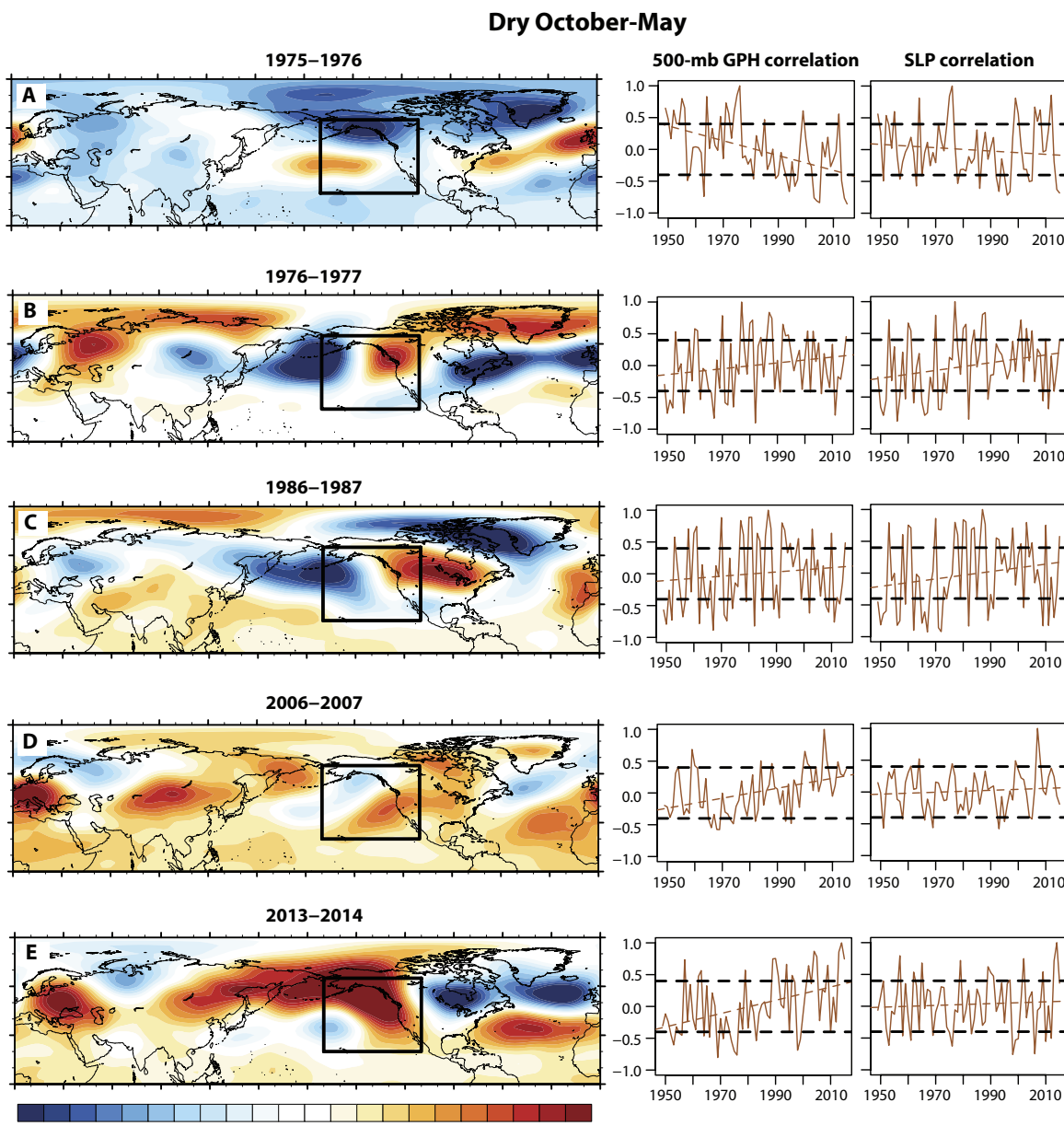


Fig. 3. Trends in California extreme dry patterns. (A to E) October–May 500-mb GPH anomaly patterns during California’s five driest cool-season periods between 1949 and 2015 (left column) and time series of pattern correlation between GPH/SLP in each specific year of interest (right column) and all other years. Horizontal dashed black lines highlight ± 0.4 correlation thresholds used to define “moderate to high correlation” in this study. Maps shown are October–May 500-mb GPH anomalies for the given year (meters).

Previous work has highlighted California's dependence on a relatively small number of storm events for the bulk of its annual precipitation, and found that California's driest and wettest years occur primarily as a result of variations in the frequency of the strongest individual storms (11, 12). Our findings are consistent with the notion that persistent, seasonal-scale anomalies in northeastern Pacific atmospheric circulation cause California's driest and wettest years by modulating the frequency and/or trajectory of extratropical cyclones. We suggest that the observed heterogeneity of NPD GPH patterns during extreme dry years may result from multiple distinct seasonal-scale atmospheric forcing regimes,

whereas the uniformity of negative GPH anomalies during extreme wet years indicates a more common etiology. These considerations become especially relevant when attempting to infer the likelihood of changes in meteorological extremes from changes in the mean state. Such large heterogeneity in the atmospheric circulation patterns that lead to extremely low seasonal-scale precipitation strongly reinforces the importance of separately considering each pattern when assessing long-term trends, particularly for the case of drought.

The simulated response of California's long-term mean annual precipitation to strongly elevated (that is, "future") greenhouse forcing has

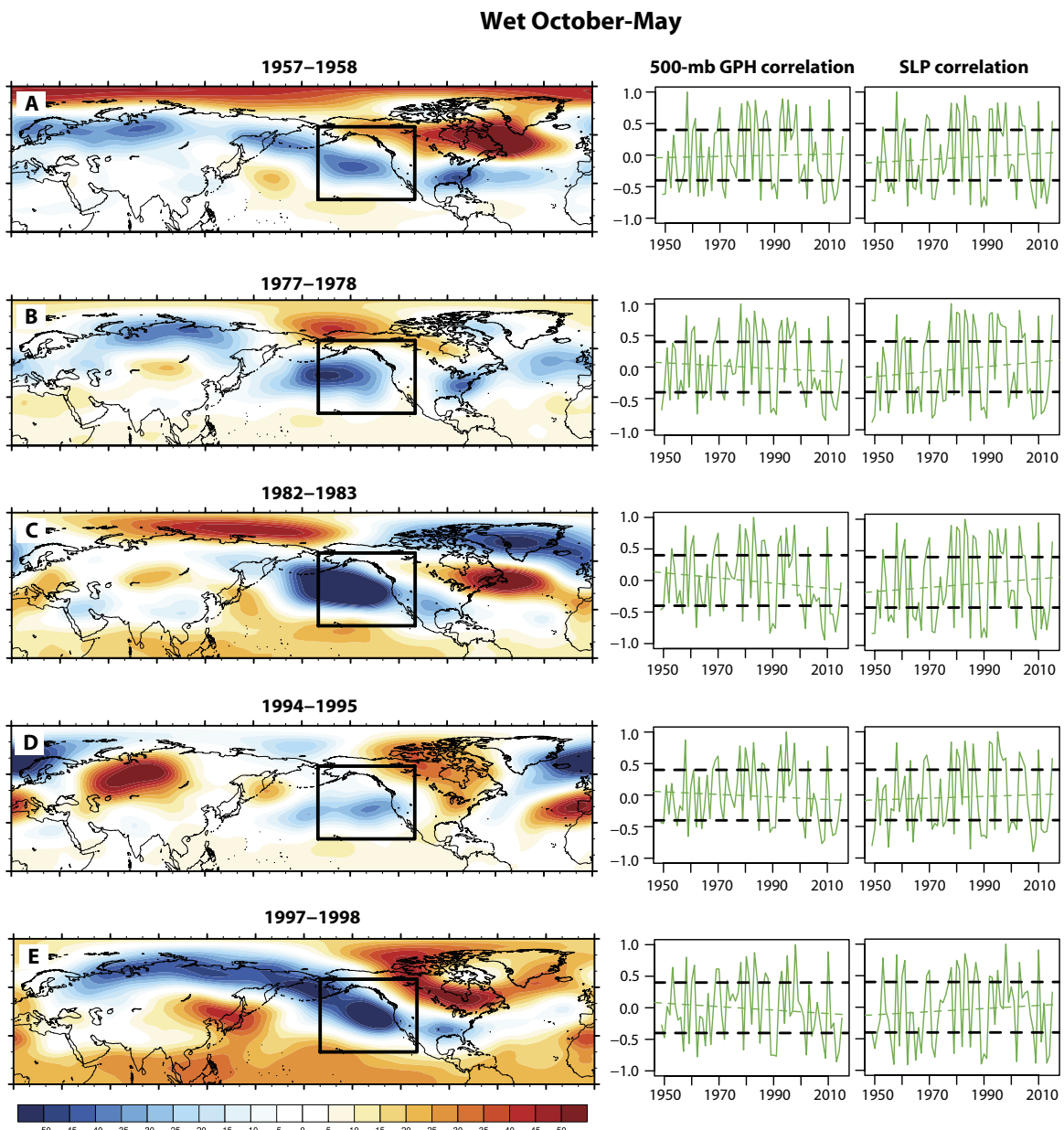


Fig. 4. Trends in California extreme wet patterns. (A to E) October–May 500-mb GPH anomaly patterns during California’s five wettest cool-season periods between 1949 and 2015 (left column) and time series of pattern correlation between GPH/SLP in each specific year of interest (right column) and all other years. Horizontal dashed black lines highlight ± 0.4 correlation thresholds used to define moderate to high correlation in this study. Maps shown are October–May 500-mb GPH anomalies for the given year (meters).

been used to argue that historical global warming has not influenced the probability of conditions that create low precipitation in California [for example, Seager *et al.* (26)]. However, coupled climate model simulations that assume a scenario of strong greenhouse forcing actually project a nuanced mix of co-occurring, physically self-consistent hydroclimatic changes in California (14, 32, 36–38). The multimodel ensemble from the Coupled Model Intercomparison Project Phase 5 (CMIP5) projects a modest increase in December–February mean precipitation (34, 39) [although it exhibits considerable intermodel disagreement (33)], and most individual models suggest a large increase

in the occurrence of extreme wet events on daily to annual time scales (31, 34–36, 40–43). Yet there is also considerable evidence that precipitation during the rest of California’s wet season (in autumn and especially spring) will decrease in response to elevated forcing (14, 36, 38) and that the likelihood of extremely dry years will increase overall (although perhaps at a lesser rate than the likelihood of extremely wet years) (14, 32, 34–36).

Proposed proximal causes of these divergent changes at either extreme of the precipitation distribution include (i) an eastward extension of the Pacific jet stream (33, 34, 39) and increased frequency/intensity

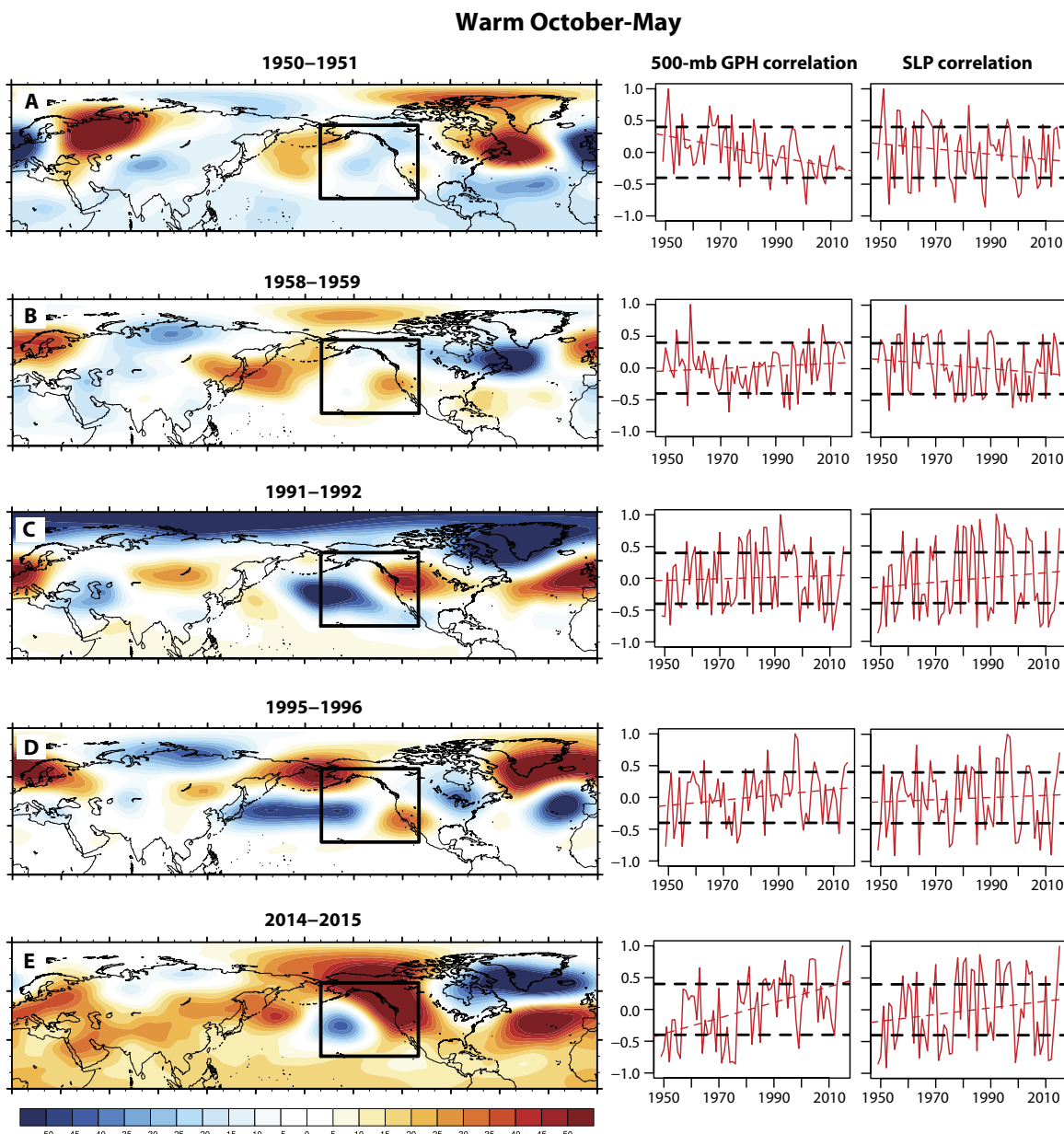


Fig. 5. Trends in California extreme warm patterns. (A to E) October–May 500-mb GPH anomaly patterns during California’s five warmest detrended cool-season periods between 1949 and 2015 (left column) and time series of pattern correlation between GPH/SLP in each specific year of interest (right column) and all other years. Horizontal dashed black lines highlight ± 0.4 correlation thresholds used to define moderate to high correlation in this study. Maps shown are October–May 500-mb GPH anomalies for the given year (meters).

of transient atmospheric rivers (leading to more wet periods) (40, 41, 44), and (ii) more frequent/intense amplification of the West Coast ridge and decreased precipitation frequency associated with northward shifts in the storm track (leading to more dry periods) (19, 27, 31, 33, 41). However, many of the atmospheric features associated with such extremes—such as persistent ridging/blocking, seasonal-scale shifts in the storm track, and relatively infrequent fine-scale events such as atmospheric rivers—are precisely the variety of phenomena that global climate models struggle to reproduce with realistic frequency and structure, lending considerable uncertainty to 21st century predictions (26, 32–34).

The results presented here further highlight the critical importance of considering changes in the occurrence and underlying mechanisms of specific circulation patterns (both during the historical period and in the future) because these patterns may substantially differ in character and surface meteorological impacts from changes in the mean state [for example, Simpson *et al.* (45)], and may not respond linearly to increasing climate forcing.

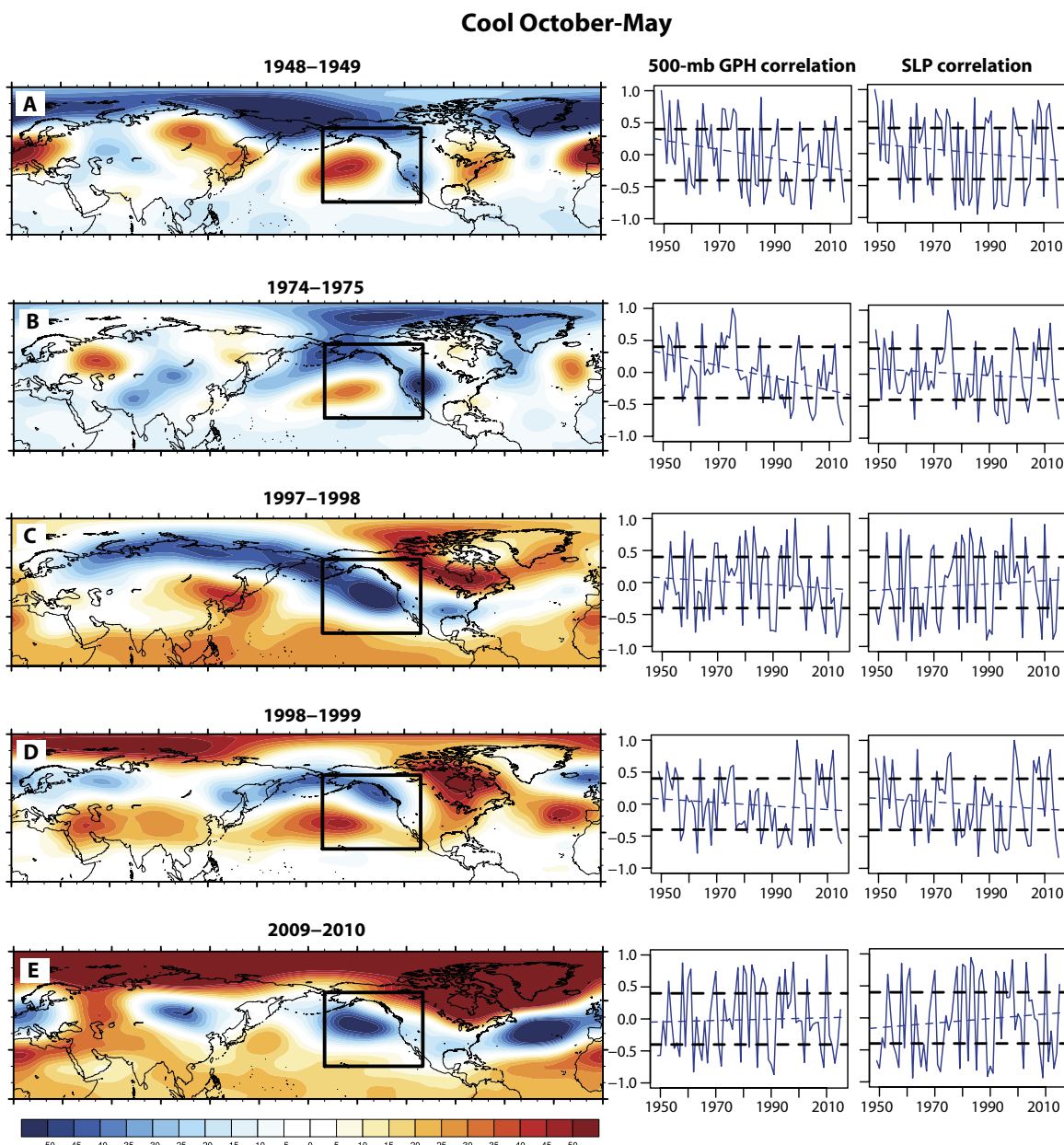


Fig. 6. Trends in California extreme cool patterns. (A to E) October-May 500-mb GPH anomaly patterns during California's five coolest detrended cool-season periods between 1949 and 2015 (left column) and time series of pattern correlation between GPH/SLP in each specific year of interest (right column) and all other years. Horizontal dashed black lines highlight ± 0.4 correlation thresholds used to define moderate to high correlation in this study. Maps shown are October-May 500-mb GPH anomalies for the given year (meters).

Increased frequency of atmospheric patterns similar to those experienced during the 2012–2015 California drought

We note that the spatial character and magnitude of the extreme mid-tropospheric wave patterns over the northeastern Pacific and North America during 2013–2014 and 2014–2015 were strikingly similar, with cyclonic anomalies over the central North Pacific just north of Hawaii, a high-amplitude ridge along, or just west, of the coastline of western North America, and a deep trough further east over Hudson Bay (Figs. 3E and 5E). Both of these years yielded very dry and very warm conditions in California, which, combined with antecedent dryness and warmth, produced 3-year October–May precipitation deficits and 3-year October–May temperature values unprecedented in the state's 119-year observational record (fig. S10, B and C). The extraordinary magnitude of this high-amplitude atmospheric pattern in recent winters has tentatively been linked to several distinct surface forcings—including anomalously warm tropical sea surface temperatures (20, 21, 27) and anomalously low Arctic sea ice extent (22, 25)—although a considerable contribution was likely also made by random atmospheric variability (26). Long-term increases in the particular Pacific sea surface temperature pattern associated with this persistent ridging have been observed; although there is evidence that the signal may be anthropogenically forced (20, 27, 46), distinguishing this trend from natural decadal variability (21, 47) and/or possible midlatitude ocean-atmosphere feedbacks (23, 48) has proven difficult. Further complicating the overall picture is recent evidence suggesting that the atmospheric response to declining sea ice may be highly sensitive to the spatial pattern of ice loss and that decreasing coverage in the Pacific sector (that is, the East Siberian/Chukchi Sea region) may be especially influential in driving large-scale atmospheric shifts over North America (25). Recent work has shown that recent drought years in California have coincided with a significant reduction in storm frequency associated with an increase in anticyclone intensity and persistence over the northeastern Pacific (49). Some have argued that an increase in the persistence of regional circulation patterns may be linked to enhanced high-latitude warming (that is, Arctic amplification) and/or sea ice loss (50, 51), although this topic remains the subject of vigorous ongoing discussion.

Additional uncertainty arises from the potentially opposing influences of Arctic and tropical warming on the midlatitude circulation. For instance, Barnes and Polvani (52) found that although the degree of simulated future Arctic amplification is significantly related to changes in several key atmospheric indicators across the American sector, this effect is apparently muted (or even reversed) by other competing large-scale influences. This emerging dynamical “tug of war” (52, 53)—and the fact that the individual contributions of specific forcings may reinforce or oppose each other in different regions and/or seasons (38, 45, 54)—highlights the inherent challenges in identifying causal influences of specific patterns using observational data alone. Therefore, we reiterate that the present study does not explicitly identify the underlying causes of the observed northeastern Pacific circulation trends. However, the demonstrated anthropogenic contribution to Arctic sea ice loss (55) and to the spatial pattern of SST warming in the Pacific (46), coupled with our finding of robust increases in North Pacific atmospheric circulation patterns that are similar to that observed in 2014–2015 (Fig. 5E), suggests that these dynamical mechanisms should be explored further within a formal climate change attribution framework.

Using such a framework, Swain *et al.* (19) attributed the 20th century increase in extreme annual-scale GPH over the northeastern Pacific to

anthropogenic greenhouse gas emissions. However, Swain *et al.* did not make specific attribution claims regarding the particular anomalous spatial configuration exhibited by the Ridiculously Resilient Ridge. Although we have not used a formal attribution framework in the current study, we do note that (i) the 1949–2015 mean trend in GPH and SLP over the far northeastern Pacific (Fig. 1A) strongly resembles the circulation pattern observed during the latter half of the 2012–2015 California drought (Figs. 3E and 5E); (ii) the increasing trend in West Coast ridging patterns similar to that observed in 2014–2015 is robust to domain-mean GPH detrending (figs. S8 and S9) as well as the use of SLP in place of GPH (Figs. 1, F and G, and 5E); (iii) years with high correlation with the observed 2014–2015 pattern appear to be preferentially driving the long-term increasing trend in GPH (fig. S10A); and (iv) the pattern and magnitude of the long-term trend in GPH are caused primarily by the pattern of direct thermal dilation (Fig. 1, A and B, and fig. S1). The results presented in the current study therefore confirm that the observed pattern of the long-term GPH trend in the NPD is spatially nonuniform, strongly positive in the mean, driven by the specific pattern of lower tropospheric warming, and characterized by an amplification of the West Coast mean ridge highly reminiscent of that which occurred during historical dry and warm years in California.

These empirical findings demonstrate a complex evolution over the northeastern Pacific between 1949 and 2015, with 500-mb GPH and SLP trends of generally the same sign occurring “in-phase” with the mean West Coast cool-season ridge (Fig. 1, A to C, and fig. S1) and the largest trends occurring just east of the terminus of the East Pacific storm track (33). This is especially interesting in light of recent investigations into the physical structure of anthropogenically forced trends in regional atmospheric circulation, which have suggested that changes in mean flow (via momentum/energy fluxes driven by embedded transient cyclones) may reinforce planetary-scale stationary waves in the upper atmosphere under certain conditions (37, 45, 54, 56). Additionally, because the location and amplitude of atmospheric stationary waves are dictated by the relative placement and orography of global landmasses, the observed alignment of the nonuniform spatial pattern of thermal dilation with the North American continent (Fig. 1B) supports the notion that at least some of the observed trend in GPH—and thus specific extreme atmospheric configurations—may be due to increasing land-sea thermal contrasts. Enhanced warming over the continents is a predicted (and observed) response to global greenhouse forcing and has the potential to influence broader circulation regimes (57, 58). Ultimately, our observational findings support model-based arguments that the net circulation response to global warming across the northeastern Pacific may be shaped by complex, regionally specific interactions between the climatological mean wave pattern and atmospheric variability on both subseasonal and interannual time scales.

Contribution of circulation changes to California’s cool-season temperature extremes

The actual (that is, not detrended) occurrence of seasonal-scale warm temperature extremes in California has dramatically increased over the 1949–2015 period (fig. S10C). This increase has largely been attributed to the thermodynamic contribution of global warming (14). However, the fact that we still find increased occurrence of atmospheric patterns associated with extreme warmth using GPH, detrended GPH, and SLP (Figs. 1, F and G, and 5 and fig. S8) suggests the potential for an additional contribution from trends in large-scale atmospheric circulation patterns that has further increased the likelihood of anomalously warm

October–May periods. In contrast, we find only one statistically significant decrease in spatial patterns associated with extremely cool years using GPH (Figs. 1F and 6), and none using SLP (Figs. 1G and 6), despite a large decrease in the actual occurrence of cool years (fig. S10B). The fact that “cool” circulation patterns are still occurring with essentially unchanged frequency (Fig. 6), but the cold temperatures themselves are not, suggests that the observed warming at the lower end of the temperature distribution primarily stems from thermodynamic warming (as opposed to trends in circulation). These results are broadly consistent with findings regarding the contribution of trends in circulation patterns to observed changes in the frequency of daily-scale hot and cold extremes in other parts of the Northern Hemisphere [for example, Horton *et al.* (30)].

Concluding remarks

We have analyzed the occurrence of large-scale atmospheric circulation patterns associated with seasonal-scale precipitation and temperature extremes in California. We find that the occurrence of several such patterns has changed significantly in recent decades. In particular, we find robust increases (using both GPH- and SLP-based metrics) in the occurrence of patterns similar to those experienced during the latter half of the ongoing severe California drought, which has been characterized by a persistent ridge near the West Coast of North America, leading to both extremely low precipitation (2013–2014) and extremely warm temperatures (2014–2015). Further, despite little observed change in GPH-based metrics for patterns linked to extremely wet years, our analysis demonstrates an increase in wet SLP patterns. Together, these findings are suggestive of a possible increase in regional variance of large-scale patterns linked to surface precipitation extremes in California.

In addition to these observed changes in specific extreme atmospheric configurations, we also find a multidecadal trend toward amplification of the mean cool-season state over the North Pacific, resulting in a stronger ridge near the West Coast of North America. The proximal cause of these observed trends appears to be the superposition of a strikingly nonuniform pattern of lower tropospheric thermal dilation and in-phase SLP changes, which favor more persistent and/or frequent midtropospheric ridging patterns over the far northeastern Pacific.

We suggest that California and the adjacent northeastern Pacific make an excellent test bed for investigations of the physical processes governing regional climate change. Given the large interannual variability of the northeastern Pacific, the existence of potentially competing dynamic and thermodynamic contributions to circulation trends (41), and the complex seasonal expressions of observed and projected future changes (33, 45), detecting and understanding the mechanisms underlying climate shifts in this region require targeted approaches that explicitly account for intrinsic climatological subtleties. Radiatively forced changes in climate are thought to preferentially reinforce natural modes of variability (29, 59); therefore, we suggest that investigations focusing on regions like California—which exhibit well-defined circulation anomalies associated with surface meteorological extremes—may be particularly enlightening (60). Further, our approach is also readily transferable to other regions and therefore provides a more general framework for understanding linkages between large-scale atmospheric patterns and regional climate change.

Managing the socioeconomic and environmental impacts of extreme meteorological events in California is a challenging endeavor (18). In many cases, natural hazard risks of opposing character—such

as droughts and floods—must be dealt with simultaneously. The situation during the present 2015–2016 wet season provides a stark example of this conundrum: in the midst of California’s record-breaking drought, a very strong El Niño event in the tropical Pacific Ocean holds the potential to disrupt persistent multi-year ridging across the northeastern Pacific and bring drought-alleviating precipitation (and perhaps even an increased risk of flooding and mudslides). However, as of March 2016, El Niño has thus far delivered only modest drought relief—which will undoubtedly raise further questions regarding the character and causes of the resilient West Coast ridge. Together, the physical complexity and acute impacts of these hydroclimatic conditions demonstrate the critical importance of understanding changes in the spatial and temporal characteristics of specific large-scale atmospheric patterns that lead to surface meteorological extremes.

MATERIALS AND METHODS

Experimental design

We used monthly 500-mb GPH and SLP data from the NCEP/NCAR R1 Reanalysis [a joint project between the National Centers for Environmental Prediction (NCEP)/National Center for Atmospheric Research (NCAR)] (61) to characterize large-scale, midtropospheric atmospheric conditions. We used monthly precipitation and temperature data from the NCDC nClimDiv climate divisional data set (for the full state of California) to assess the extremity of surface meteorological conditions (available at www.ncdc.noaa.gov/monitoring-references/maps/us-climate-divisions.php). Whereas the NCDC precipitation and temperature data sets extend as far back as 1895, the R1 reanalysis begins in 1948, and so we restricted our analysis to the overlapping set of full October–May “cool season” periods between 1949 and 2015 (October 1948 through May 1949, October 1949 through May 1950, etc). Our analysis encompassed an approximately rectangular geographic domain (20°N – 65°N , 190°E – 250°E) extending from the central North Pacific basin west to the central Rocky Mountains over the North American continent. We refer to this area of analysis as the NPD.

Analysis of precipitation and temperature data

To identify extreme years in the observed record, we calculated 8-month (October–May) mean values for both precipitation and temperature. We then selected the five highest values from each variable and respectively defined them as the “extreme wet” and “extreme warm” years, and the five lowest values from each variable and respectively defined them as the “extreme dry” and “extreme cool” years. (Given that there are 67 years in our historical period of record, these represent the top and bottom 7.5% of the temperature and precipitation distributions.) Here, we sought to test hypotheses about changes in precipitation and temperature associated with changes in the atmospheric circulation. Because of a pronounced long-term warming trend in California (14) (fig. S10C), we fit a linear model to the temperature data and removed the time-mean trend before calculating the five warmest and five coolest years. Failure to remove the observed increasing trend in October–May mean temperature would bias our extreme event analysis toward recent years that could have been made extreme by the long-term thermodynamic trend rather than by large deviations in the atmospheric conditions during those years (that is, all of California’s top five warmest years on record have occurred since 1990; fig. S10C). In contrast, because

there has been little if any trend in mean cool-season precipitation in California (14) (fig. S10CB), we used the raw precipitation data to calculate the five driest and five wettest years.

Analysis of GPH and SLP data

We first calculated 8-month (October–May) mean values for midtropospheric (500 mb) GPHs for each grid point in the Northern Hemisphere. We then created a three-dimensional (year \times latitude \times longitude) anomaly time series by subtracting the mean 1949–2015 October–May value from the yearly October–May value at each grid point for each of the 67 years. From this three-dimensional GPH anomaly time series, we selected the GPH field associated with each of the 20 extreme dry/wet/warm/cool years. Lastly, for each of these 20 extreme-year GPH maps, we calculated the pattern correlation between the respective extreme-year GPH anomaly map and the anomaly map of each of the 67 years in the GPH anomaly time series, yielding 20 time series of pattern correlation. We repeated this process using SLP, yielding a further 20 time series of pattern correlation. We present the GPH- and SLP-derived findings side by side in the text.

To assess changes in the cool-season mean state over the northeastern Pacific Ocean and adjacent western North America, we calculated, for each year, the October–May mean zonal gradient of NPD GPH over four separate latitude bands (using the original, non-detrended GPH field). The reported zonal gradients were derived by calculating the area-weighted mean of west-to-east finite differences in GPH at each grid point within each latitude band and then summing over all longitudes within the NPD. This yielded four 67-year time series of the mean October–May zonal GPH gradient in each latitude band. For each band, we reported both the linear mean trend and changes in high/low (± 1 SD) cool-season gradients between the first half (1949–1981) and the second half (1982–2015) of the historical period of record. Using the method described above, we performed further analysis of subseasonal data to calculate the mean GPH gradient during each calendar month between May and October for the 1949–2015 period. We then created a month-by-month mean “climatology” to report departures from month-specific mean values in each latitude band. We measured the persistence of the monthly GPH gradient by counting the mean number of consecutive months in each October–May season during which the GPH gradient exceeded the long-term month-specific mean, and reported a single value for each year.

Partitioning direct thermal and dynamical contributions to observed GPH trend

The thermal dilation effect of global warming is expected to increase the mean GPH of constant-pressure surfaces across the Northern Hemisphere (62), although the actual observed changes have been strongly heterogeneous (30). To test the sensitivity of the occurrence of large-scale 500-mb GPH to uniform increases in the mean field (rather than changes in the spatial pattern or the horizontal gradient), we repeated the GPH analysis described in the previous section by first calculating and removing the domain-mean linear trend (0.289 m/year) from each grid point in the NPD domain. This approach implicitly controls for the regional-mean trend while preserving any spatially heterogeneous trends that might exist (full results shown in the Supplementary Materials).

However, the substantial spatial heterogeneity in the observed GPH trends suggests that the regional-mean trend may be due to a combination of nonuniform thermal dilation and changes in the large-scale cir-

culation (30) and that removal of the observed GPH trend may not be a valid assumption. We therefore performed additional analysis to explore the causes of the observed spatially heterogeneous GPH trends. To quantify the relative contributions of lower tropospheric thermal dilation and SLP change on GPH, we partitioned the GPH trend using Li *et al.*'s (63) hydrostatic approximation approach. Using monthly temperature data from the surface through 500 mb, we calculated the expected contribution of thermal expansion (or contraction) to changes in the height of the 500-mb pressure surface at each grid box in the Northern Hemisphere. We performed an analogous calculation for SLP to quantify the expected contribution of dynamical trends (that is, changes in local air column mass) to changes in the height of the 500-mb surface. We show the partitioned contributions for the entire North Pacific basin and the continent of North America in Fig. 1 and fig. S1, but focus on results within the NPD in the text.

Statistical analysis

We calculated linear trends for zonal-mean October–May GPH gradients. All trends were calculated by fitting a linear least squares regression to the data, and *P* values signified the confidence that the regression coefficients for each model were statistically significant using a two-tailed test. The sign and significance of GPH gradient trends may be interpreted as answering the question, “Is there a statistically significant long-term trend toward amplification of the October–May mean atmospheric state over the NPD?” Additionally, we compared the frequency of occurrence of high- and low-gradient October–May seasons in the first and second halves of the observational record using a standard two-tailed *t* test to formalize confidence in the mean sign changes. We used a two-tailed *t* test to report *P* values for changes in subseasonal persistence of the zonal gradient between the two halves of the observational record. Similarly, we used a Kolmogorov-Smirnov test to determine whether the difference in distributions between seasonal mean GPH gradients for the 1949–1981 and 1982–2015 periods was statistically distinguishable. The associated *P* values are reported in Fig. 2C.

We also assessed the change in frequency of years that exhibited moderate to high correlation with the GPH or SLP pattern exhibited in the extreme dry/wet/warm/cool years. This metric may be interpreted as answering the question, “Are there changes in the occurrence of spatial patterns that are very similar those observed during the occurrence of extreme temperature or precipitation conditions?” To do so, we calculated the number of years between 1949–1981 and 1982–2015 that had pattern correlations greater than 0.4 (or less than -0.4). *P* values associated with the reported changes in moderate- to high-correlation years were derived using a conditional one-tailed binomial test predicated on a null hypothesis that the probability of occurrence of specific patterns is the same during 1982–2015 and during 1949–1981 [that is, assuming stationarity in the frequency of circulation patterns, and using an upper (lower) tailed test if the observed change is positive (negative)]. In this case, rejection of the null suggested that the observed increase (or decrease) in pattern frequency was very unlikely to have occurred by chance.

To confirm that GPH/SLP pattern correlations exceeding the >0.4 and <-0.4 thresholds were useful predictors of actual extreme surface metrological outcomes in California, we calculated the fraction of years with high positive (negative) correlations that exhibited precipitation/temperature anomalies of the correct sign for each year type. We considered a particular pattern correlation to have “correctly identified” increased likelihood of an extreme year when the fraction of years was

greater than 60%. For example, for each extreme dry GPH/SLP map, we first identified all the years from 1949 to 2015 in which the October–May GPH map exhibited >0.4 correlation with that extreme dry GPH/SLP map. We then calculated the fraction of those identified years in which precipitation was actually below the long-term mean (which, in this case, was greater than 60% for four of five patterns). Here, as before, we used the raw precipitation data and the linearly detrended temperature data, calculating anomalies relative to the mean for the full period of record (1949–2015).

A P value of <0.10 was considered statistically significant. P values are also reported in the figures so that significance can be evaluated on a case-by-case basis.

SUPPLEMENTARY MATERIALS

Supplementary material for this article is available at <http://advances.sciencemag.org/cgi/content/full/2/4/e1501344/DC1>

Fig. S1. Observed October–May changes across the northeastern Pacific.

Fig. S2. Observed October–May changes in zonal GPH gradient over the northeastern Pacific.

Fig. S3. Trends in California extreme dry patterns.

Fig. S4. Trends in California extreme wet patterns.

Fig. S5. Trends in California extreme warm patterns.

Fig. S6. Trends in California extreme cool patterns.

Fig. S7. Change in frequency of high-correlation years using GPH.

Fig. S8. A comprehensive summary of extreme pattern trend results for analysis using linearly detrended 500-mb GPH data (columns labeled “DT”) and using non-detrended GPH data (columns labeled “NDT”).

Fig. S9. Time series of pattern correlation between GPH pattern in each specific year of interest and all other years using linearly detrended GPH data.

Fig. S10. Observed trends in GPH, precipitation, and temperature.

REFERENCES AND NOTES

- J. A. Screen, I. Simmonds, Amplified mid-latitude planetary waves favour particular regional weather extremes. *Nat. Clim. Change* **4**, 704–709 (2014).
- E. K. Wise, M. P. Dannenberg, Persistence of pressure patterns over North America and the North Pacific since AD 1500. *Nat. Commun.* **5**, 4912 (2014).
- A. F. Van Loon, E. Tijdeman, N. Wanders, H. A. J. Van Lanen, A. J. Teuling, R. Uijlenhoet, How climate seasonality modifies drought duration and deficit. *J. Geophys. Res.-Atmos.* **119**, 4640–4656 (2014).
- United States Census Bureau. *California Quick Facts* (2015); <http://quickfacts.census.gov/qfd/states/06000.html> [accessed 8 March 2016].
- California Legislative Analyst's Office. *California is the World's 8th Largest Economy* (2015); www.lao.ca.gov/LAOEconTax/Article/Detail/1 [accessed 8 March 2016].
- United States Department of Agriculture. *California Agricultural Statistics 2012 Crop Year* (2014); www.nass.usda.gov/Statistics_by_State/California/Publications/California_Ag_Statistics/Reports/2012cas-all.pdf [accessed 8 March 2016].
- N. Myers, R. A. Mittermeier, C. G. Mittermeier, G. A. B. da Fonseca, J. Kent, Biodiversity hotspots for conservation priorities. *Nature* **403**, 853–858 (2000).
- California Protected Areas Database. *California Protected Areas Data Portal* (2015); www.calands.org/uploads/docs/cpad_flyer.pdf [accessed 8 March 2016].
- D. R. Cayan, J. O. Roads, Local relationships between United States West Coast precipitation and monthly mean circulation parameters. *Mon. Weather Rev.* **112**, 1276–1282 (1984).
- R. W. Higgins, Y. Yao, X. L. Wang, Influence of the North American Monsoon System on the U.S. summer precipitation regime. *J. Climate* **10**, 2600–2622 (1997).
- M. D. Dettinger, F. M. Ralph, T. Das, P. J. Neiman, D. R. Cayan, Atmospheric rivers, floods and the water resources of California. *Water* **3**, 445–478 (2011).
- M. D. Dettinger, Atmospheric rivers as drought busters on the U.S. West Coast. *J. Hydrometeorol.* **14**, 1721–1732 (2013).
- D. Griffin, K. J. Anchukaitis, How unusual is the 2012–2014 California drought? *Geophys. Res. Lett.* **41**, 9017–9023 (2014).
- N. S. Diffenbaugh, D. L. Swain, D. Touma, Anthropogenic warming has increased drought risk in California. *Proc. Natl. Acad. Sci. U.S.A.* **112**, 3931–3936 (2015).
- S. M. Robeson, Revisiting the recent California drought as an extreme value. *Geophys. Res. Lett.* **42**, 6771–6779 (2015).
- A. Aghakouchak, L. Cheng, O. Mazdiyasni, A. Farahmand, Global warming and changes in risk of concurrent climate extremes: Insights from the 2014 California drought. *Geophys. Res. Lett.* **41**, 8847–8852 (2014).
- A. P. Williams, R. Seager, J. T. Abatzoglou, B. I. Cook, J. E. Smerdon, E. R. Cook, Contribution of anthropogenic warming to California drought during 2012–2014. *Geophys. Res. Lett.* **42**, 6819–6828 (2015).
- D. L. Swain, A tale of two California droughts: Lessons amidst record warmth and dryness in a region of complex physical and human geography. *Geophys. Res. Lett.* **42**, 9999–10003 (2015).
- D. L. Swain, M. Tsiang, M. Haugen, D. Singh, A. Charland, B. Rajaratnam, N. S. Diffenbaugh, The extraordinary California drought of 2013/2014: Character, context, and the role of climate change. *Bull. Am. Meteorol. Soc.* **95**, S3–S7 (2014).
- S.-Y. Wang, L. Hipps, R. R. Gillies, J.-H. Yoon, Probable causes of the abnormal ridge accompanying the 2013–2014 California drought: ENSO precursor and anthropogenic warming footprint. *Geophys. Res. Lett.* **41**, 3220–3226 (2014).
- D. L. Hartmann, Pacific sea surface temperature and the winter of 2014. *Geophys. Res. Lett.* **42**, 1894–1902 (2015).
- M.-Y. Lee, C.-C. Hong, H.-H. Hsu, Compounding effects of warm sea surface temperature and reduced sea ice on the extreme circulation over the extratropical North Pacific and North America during the 2013–2014 boreal winter. *Geophys. Res. Lett.* **42**, 1612–1618 (2015).
- C. Funk, A. Hoell, D. Stone, Examining the contribution of the observed global warming trend to the California droughts of 2012/13 and 2013/14. *Bull. Am. Meteorol. Soc.* **95** (Special Suppl. 9), S11–S15 (2014).
- J. O. Sewall, L. C. Sloan, Disappearing Arctic sea ice reduces available water in the American west. *Geophys. Res. Lett.* **31**, L06209 (2005).
- J.-S. Kug, J.-H. Jeong, Y.-S. Jang, B.-M. Kim, C. K. Folland, S.-K. Min, S.-W. Son, Two distinct influences of Arctic warming on cold winters over North America and East Asia. *Nat. Geosci.* **8**, 759–762 (2015).
- R. Seager, M. Hoerling, S. Schubert, H. Wang, B. Lyon, A. Kumar, J. Nakamura, N. Henderson, Causes of the 2011–14 California Drought. *J. Climate* **28**, 6997–7024 (2015).
- S.-Y. S. Wang, W.-R. Huang, J.-H. Yoon, The North American winter ‘dipole’ and extremes activity: A CMIP5 assessment. *Atmosph. Sci. Lett.* **16**, 338–345 (2015).
- T. Palmer, Record-breaking winters and global climate change. *Science* **344**, 803–804 (2014).
- T. G. Shepherd, Atmospheric circulation as a source of uncertainty in climate change projections. *Nat. Geosci.* **7**, 703–708 (2014).
- D. E. Horton, N. C. Johnson, D. Singh, D. L. Swain, B. Rajaratnam, N. S. Diffenbaugh, Contribution of changes in atmospheric circulation patterns to extreme temperature trends. *Nature* **522**, 465–469 (2015).
- S. D. Polade, D. W. Pierce, D. R. Cayan, A. Gershunov, M. D. Dettinger, The key role of dry days in changing regional climate and precipitation regimes. *Sci. Rep.* **4**, 4364 (2014).
- D. W. Pierce, D. R. Cayan, T. Das, E. P. Maurer, N. L. Miller, Y. Bao, M. Kanamitsu, K. Yoshimura, M. A. Snyder, L. C. Sloan, G. Franco, M. Tyree, The key role of heavy precipitation events in climate model disagreements of future annual precipitation changes in California. *J. Climate* **26**, 5879–5896 (2013).
- B. Langenbrunner, J. D. Neelin, B. R. Lintner, B. T. Anderson, Patterns of precipitation change and climatological uncertainty among CMIP5 Models, with a focus on the mid-latitude Pacific storm track. *J. Climate* **28**, 7857–7872 (2015).
- N. Berg, A. Hall, Increased interannual precipitation extremes over California under climate change. *J. Climate* **28**, 6324–6334 (2015).
- J.-H. Yoon, S.-Y. S. Wang, R. R. Gillies, B. Kravitz, L. Hipps, P. J. Rasch, Increasing water cycle extremes in California and in relation to ENSO cycle under global warming. *Nat. Commun.* **6**, 8657 (2015).
- N. S. Diffenbaugh, F. Giorgi, Climate change hotspots in the CMIP5 global climate model ensemble. *Clim. Change* **114**, 813–822 (2012).
- I. R. Simpson, R. Seager, M. Ting, T. A. Shaw, Causes of change in Northern Hemisphere winter meridional winds and regional hydroclimate. *Nat. Clim. Change* **6**, 65–70 (2016).
- R. Seager, D. Neelin, I. Simpson, H. Liu, N. Henderson, T. Shaw, Y. Kushnir, M. Ting, B. Cook, Dynamical and thermodynamical causes of large-scale changes in the hydrological cycle over North America in response to global warming. *J. Climate* **27**, 7921–7948 (2014).
- J. D. Neelin, B. Langenbrunner, J. E. Meyerson, A. Hall, N. Berg, California winter precipitation change under Global Warming in the Coupled Model Intercomparison Project Phase 5 ensemble. *J. Climate* **26**, 6238–6256 (2013).
- D. A. Lavers, F. M. Ralph, D. E. Waliser, A. Gershunov, M. D. Dettinger, Climate change intensification of horizontal water vapor transport in CMIP5. *Geophys. Res. Lett.* **42**, 5617–5625 (2015).
- Y. Gao, J. Lu, L. R. Leung, Q. Yang, S. Hagos, Y. Qian, Dynamical and thermodynamical modulations on future changes of landfalling atmospheric rivers over western North America. *Geophys. Res. Lett.* **42**, 7179–7186 (2015).
- V. V. Kharin, F. W. Zwiers, X. Zhang, M. Wehner, Changes in temperature and precipitation extremes in the CMIP5 ensemble. *Clim. Change* **119**, 345–357 (2013).

43. IPCC, *Climate Change 2014: Impacts, Adaptation, and Vulnerability. Part B: Regional Aspects. Contribution of Working Group II to the Fifth Assessment Report of the Intergovernmental Panel on Climate Change*, V. R. Barros, C. B. Field, D. J. Dokken, M. D. Mastrandrea, K. J. Mach, T. E. Bilir, M. Chatterjee, K. L. Ebi, Y. O. Estrada, R. C. Genova, B. Girma, E. S. Kissel, A. N. Levy, S. MacCracken, P. R. Mastrandrea, and L. L. White Eds. (Cambridge Univ. Press, Cambridge, 2014), 688 pp.
44. M. Dettinger, Climate change, atmospheric rivers, and floods in California—A multimodel analysis of storm frequency and magnitude changes. *J. Am. Water Resour. As.* **47**, 514–523 (2011).
45. I. R. Simpson, T. A. Shaw, R. Seager, A diagnosis of the seasonally and longitudinally varying midlatitude circulation response to Global Warming. *J. Atmos. Sci.* **71**, 2489–2515 (2014).
46. C. C. Funk, A. Hoell, The leading mode of observed and CMIP5 ENSO-residual sea surface temperatures and associated changes in Indo-Pacific climate. *J. Climate* **28**, 4309–4329 (2015).
47. T. L. Delworth, F. Zeng, A. Rosati, G. A. Vecchi, A. T. Wittenberg, A link between the hiatus in Global Warming and North American drought. *J. Climate* **28**, 3834–3845 (2015).
48. N. A. Bond, M. F. Cronin, H. Freeland, N. Mantua, Causes and impacts of the 2014 warm anomaly in the NE Pacific. *Geophys. Res. Lett.* **42**, 3414–3420 (2015).
49. J. Lehmann, D. Coumou, The influence of mid-latitude storm tracks on hot, cold, dry and wet extremes. *Sci. Rep.* **5**, 17491 (2015).
50. J. A. Francis, S. J. Vavrus, Evidence linking Arctic amplification to extreme weather in mid-latitudes. *Geophys. Res. Lett.* **39**, L06801 (2012).
51. J. A. Francis, S. J. Vavrus, Evidence for a wavier jet stream in response to rapid Arctic warming. *Environ. Res. Lett.* **10**, 014005 (2015).
52. E. A. Barnes, L. M. Polvani, CMIP5 projections of Arctic amplification, of the North American/North Atlantic circulation, and of their relationship. *J. Climate* **28**, 5254–5271 (2015).
53. I. M. Held, Large-scale dynamics and Global Warming. *Bull. Am. Meteorol. Soc.* **74**, 228–241 (1993).
54. E. A. Barnes, D. W. J. Thompson, Comparing the roles of barotropic versus baroclinic feedbacks in the atmosphere's response to mechanical forcing. *J. Atmos. Sci.* **71**, 177–194 (2014).
55. J. C. Stroeve, V. Kattsov, A. Barrett, M. Serreze, T. Pavlova, M. Holland, W. N. Meier, Trends in Arctic sea ice extent from CMIP5, CMIP3 and observations. *Geophys. Res. Lett.* **39**, L16502 (2012).
56. V. Petoukhov, S. Rahmstorf, S. Petri, H. J. Schellnhuber, Quasiresonant amplification of planetary waves and recent Northern Hemisphere weather extremes. *Proc. Natl. Acad. Sci. U.S.A.* **110**, 5336–5341 (2013).
57. S. Corti, F. Molteni, T. N. Palmer, Signature of recent climate change in frequencies of natural atmospheric circulation regimes. *Nature* **398**, 799–802 (1999).
58. R. T. Sutton, B. Dong, J. M. Gregory, Land/sea warming ratio in response to climate change: IPCC AR4 model results and comparison with observations. *Geophys. Res. Lett.* **34**, L02701 (2007).
59. T. N. Palmer, A nonlinear dynamical perspective on climate prediction. *J. Climate* **12**, 575–591 (1999).
60. S.-P. Xie, C. Deser, G. A. Vecchi, M. Collins, T. L. Delworth, A. Hall, E. Hawkins, N. C. Johnson, C. Cassou, A. Giannini, M. Watanabe, Towards predictive understanding of regional climate change. *Nat. Clim. Change* **5**, 921–930 (2015).
61. E. Kalnay, M. Kanamitsu, R. Kistler, W. Collins, D. Deaven, L. Gandin, M. Iredell, S. Saha, G. White, J. Woollen, Y. Zhu, A. Leetmaa, R. Reynolds, M. Chelliah, W. Ebisuzaki, W. Higgins, J. Janowiak, K. C. Mo, C. Ropelewski, J. Wang, R. Jenne, D. Joseph, The NCEP/NCAR 40-year reanalysis project. *Bull. Am. Meteorol. Soc.* **77**, 437–471 (1996).
62. E. A. Barnes, Revisiting the evidence linking Arctic amplification to extreme weather in midlatitudes. *Geophys. Res. Lett.* **40**, 4734–4739 (2013).
63. L. Li, W. Li, Y. Deng, Summer rainfall variability over the Southeastern United States and its intensification in the 21st century as assessed by CMIP5 models. *J. Geophys. Res.-Atmos.* **118**, 340–354 (2013).

Acknowledgments: We thank two anonymous reviewers for their insightful and constructive comments, which greatly improved the manuscript. We thank J. Mankin and D. Touma for thought-provoking conversations. We also thank NOAA ESRL for access to the NCEP reanalysis data and NOAA NCDC for access to the nClimDiv precipitation and temperature data. Computational resources for data processing and analysis were provided by the Center for Computational Earth and Environmental Science in the School of Earth, Energy, and Environmental Sciences at Stanford University. **Funding:** Our work was supported by fellowships from the Switzer Foundation and the ARCS (Achievement Rewards for College Scientists) Foundation to D.L.S.; NSF AGS CAREER Grant 0955283 and U.S. Department of Energy Integrated Assessment Research Program Grant DE-SC005171 to N.S.D.; and a G. J. Lieberman Fellowship to D.S. **Author contributions:** D.L.S. conceived of the study; D.L.S., D.E.H., D.S., and N.S.D. designed the analyses; D.L.S. and D.E.H. provided analysis tools; D.L.S. conducted the analyses; D.L.S. wrote the manuscript; and D.E.H., D.S., and N.S.D. provided comments and feedback. **Competing interests:** The authors declare that they have no competing interests. **Data and materials availability:** GPH data from the NCEP R1 Reanalysis are available at the NOAA ESRL Web site (www.esrl.noaa.gov/psd/data/gridded/data/ncp.reanalysis.html). Precipitation and temperature data for California are available at the NOAA NCDC Web site (www.ncdc.noaa.gov/monitoring-references/maps/us-climate-divisions.php). Code used in the analyses described in the paper may be obtained upon request by contacting the corresponding author.

Submitted 29 September 2015

Accepted 1 March 2016

Published 1 April 2016

10.1126/sciadv.1501344

Citation: D. L. Swain, D. E. Horton, D. Singh, N. S. Diffenbaugh, Trends in atmospheric patterns conducive to seasonal precipitation and temperature extremes in California. *Sci. Adv.* **2**, e1501344 (2016).

This article is published under a Creative Commons license. The specific license under which this article is published is noted on the first page.

For articles published under [CC BY](#) licenses, you may freely distribute, adapt, or reuse the article, including for commercial purposes, provided you give proper attribution.

For articles published under [CC BY-NC](#) licenses, you may distribute, adapt, or reuse the article for non-commercial purposes. Commercial use requires prior permission from the American Association for the Advancement of Science (AAAS). You may request permission by clicking [here](#).

The following resources related to this article are available online at <http://advances.sciencemag.org>. (This information is current as of October 19, 2016):

Updated information and services, including high-resolution figures, can be found in the online version of this article at:
<http://advances.sciencemag.org/content/2/4/e1501344.full>

Supporting Online Material can be found at:
<http://advances.sciencemag.org/content/suppl/2016/03/29/2.4.e1501344.DC1>

This article **cites 58 articles**, 3 of which you can access for free at:
<http://advances.sciencemag.org/content/2/4/e1501344#BIBL>